NRV commented example: ^{4}He+^{208}Pb elastic scattering

Introduction

This document describes briefly the use of the Nuclear Reaction Video Project (NRV) application for the case of elastic scattering. We will use as example the ^{4}He+^{208}Pb reaction and, to a lesser extent, the ^{6}He+^{208}Pb reaction. The link to the elastic scattering interface at the NRV website is:

http://nrv.jinr.ru/nrv/webnrv/elastic_scattering/els1.htm

1   Reminder of the optical model

In the optical model, the projectile-target interaction is described by means of an effective interaction, $U(\mathbf{R})$ (the *optical potential*). The scattering wavefunction describes the relative motion between the projectile and target is a solution of single-channel the Schrodinger equation: $[H - E]\Psi(\mathbf{R}) = 0$ where E is the CM energy. This solution is conveniently expanded in spherical harmonics. For a *central potential* (i.e. $U = U(R)$) and *ignoring intrinsic spins*, this yields:

$$\Psi(\mathbf{K}, \mathbf{R}) = \frac{1}{KR} \sum_L (2L + 1) i^L \chi_L(K, R) P_L(\cos\theta), \tag{1}$$

where θ is the angle between the incident momentum $\mathbf{K}$ and the final momentum $\mathbf{K}'$, which corresponds to the scattering angle in the c.m. frame.

The radial functions $\chi_L(K, R)$ are determined inserting this expansion into the Schrödinger equation, giving rise to an equation for each value of L,

$$\left[\frac{\hbar^2}{2\mu} \frac{d^2}{dR^2} - \frac{\hbar^2}{2\mu} \frac{L(L+1)}{R^2} - U(R) + E \right] \chi_L(K, R) = 0, \tag{2}$$

where $U(R)$ contains both the Coulomb and nuclear potentials.

The above Schrödinger equation is solved numerically from $R = 0$, starting from the value $\chi_L(K, 0) = 0$, and up to a maximum value (*matching radius*) $R_{\max}$. At this distance, one imposes the boundary condition:

$$\chi_L(K, R)|_{R=R_{\max}} = \frac{i}{2} e^{i\sigma_L} \left[H_L^{(-)}(\eta, KR_{\max}) - S_L H_L^{(+)}(\eta, KR_{\max}) \right] \tag{3}$$

where σ_L are the Coulomb phase-shifts and $H^{(\pm)}(\eta, KR)$ are the ingoing $(-)$ and outgoing $(+)$ Coulomb functions. From the condition (3), one determines the coefficients S_L (S-matrix elements) which, in turn, are used to compute the elastic scattering amplitude:

$$f(\theta) = f_C(\theta) + \frac{1}{2iK} \sum_L (2L + 1) e^{2i\sigma_L} (S_L - 1) P_L(\cos\theta) \tag{4}$$
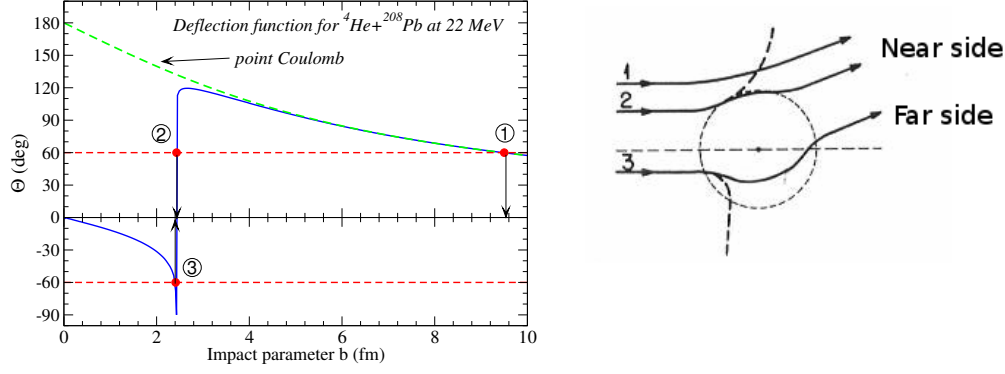
Figure 1: Left: classical deflection function. Right: classical trajectories corresponding to the impact parameters ①, ② and ③.

where $f_C(\theta)$ is the scattering amplitude for pure Coulomb scattering (whose square is the Rutherford cross section).

The differential elastic cross section is evaluated according to

$$\frac{d\sigma}{d\Omega}(\theta) = |f_C(\theta) + f_N(\theta)|^2. \tag{5}$$

An important quantity is the reaction cross section, which is associated with the flux of all non-elastic channels. In terms of the S-matrix elements it is given by:

$$\sigma_{\text{reac}} = \frac{\pi}{K^2} \sum_L (2L + 1)(1 - |S_L|^2) \tag{6}$$

where K is the wavenumber in C.M.

2   Classical description

NRV allows also a classical treatment of the reaction. For that, the code calculates the scattering angle (θ) for range of impact parameters (b). The differential elastic cross section is then computed as:

$$\frac{d\sigma}{d\Omega} = \frac{b}{\sin(\theta)}\left|\frac{db}{d\theta}\right| \tag{7}$$

If several trajectories contribute to the same scattering angle, the expression above must be replaced by

$$\frac{d\sigma}{d\Omega} = \sum_i \frac{b_i}{\sin(\theta)}\left|\frac{db}{d\Theta}\right|_i \tag{8}$$

where $\Theta(b)$ is the **classical deflection function**, which can be positive or negative corresponding respectively to the near- and far-side trajectories introduced above.

In the presence of both Coulomb and nuclear interactions, there are in general three trajectories (and hence three impact parameters) leading to the same scattering
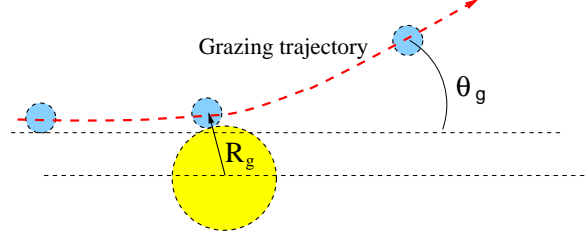
Figure 2: Classical grazing trajectory.

angle, as shown in Fig. 8: ① corresponds to a distant trajectory entirely governed by the Coulombic potential; ② corresponds to a nearside trajectory affected by both the Coulomb potential and the attractive nuclear interaction; ③ is a farside trajectory dominated by the attractive nuclear interaction.

2.1   Grazing distance, angular momentum and angle

An important quantity in the classical description of the scattering process is the *grazing distance* (R_g), defined as the projectile-target separation for which the two nuclei barely touch (see Fig. 2). If the distance of closest approach $r_{\min}$ of a given trajectory is of the order or smaller than R_g, the colliding nuclei will experience the effect of the nuclear potential. The value of R_g is found to be somewhat larger than the sum of the projectile and target radii. A simple estimate[1] is $R_g \simeq 1.45(A_p^{1/3} + A_t^{1/3})$ fm.

In Fresnel and Fraunhofer situations, there are some handy formulas relating the grazing angle, grazing angular momentum and grazing distance:

1. In **Fresnel** scattering, the grazing angle θ_g can be obtained from the quarter-point recipe: $\sigma/\sigma_R(\theta_g) = 1/4$. Then, the L_g and R_g are estimated using the following formulas valid for Coulomb trajectories:

$$L_g + 1/2 \approx \eta \cot\left(\frac{\theta_g}{2}\right) ; \qquad R_g = \frac{\eta}{k}\left(1 + \frac{1}{\sin(\theta_g/2)}\right) \tag{9}$$

2. In **Fraunhofer** scattering, the separation $\Delta\theta$ of successive maxima or minima gives a measure of the grazing angular momentum,

$$\Delta\theta \approx \pi/L_g, \tag{10}$$

and then R_g can be estimated from $k\,R_g \simeq L_g + 1/2$.

3   Optical model parameters

The projectile-target interaction is the sum of the Coulomb potential and the nuclear potential. For the Coulomb potential, NRV uses the Coulomb interaction between uniformly charged spheres:

---

[1]Other estimates can be found in the literature. For example, $R_g \simeq 0.5 + 1.36(A_p^{1/3} + A_t^{1/3})$ fm.

System	V_0 [MeV]	r_0 [fm]	a_0 [fm]	W_v [MeV]	r_i [fm]	a_i [fm]	r_c [fm]
^{4}He+^{208}Pb	96.44	1.085	0.625	32	0.958	0.42	1.2
^{6}He+^{208}Pb	124.8	1.085	0.564	6.79	0.958	1.91	1.2

Table 1: Woods-Saxon parameters for ^{4,6}He+^{208}Pb optical models. Reduced radii (r_x) are converted into absolute (physical) radii as $R_x = r_x(A_p^{1/3} + A_t^{1/3})$.

$$V_c(r) = \begin{cases} \kappa \frac{Z_1 Z_2 e^2}{2R_c} \left(3 - \frac{r^2}{R_c^2}\right) & \text{if } r \leq R_c \\ \kappa \frac{Z_1 Z_2 e^2}{r} & \text{if } r \geq R_c \end{cases}$$

where R_c is related to the sum of the charge radii of the colliding nuclei. Instead of using R_c directly, NRV uses the so-called reduced radius, r_c, which is related to the physical radius as $R_c = r_c(A_1^{1/3} + A_2^{1/3})$. In our working example $A_1 = 4$ and $A_2 = 208$.

For the nuclear part, we consider the following parametrization in terms of *volume* Woods-Saxon shapes, which is in fact the standard choice in NRV:

$$U_{\text{nuc}}(r) = -V_0 f(r, R_0, a_0) - iW_v f(r, R_i, a_i),$$

with

$$f(r, R_x, a_x) = \{1 + \exp\left[(r - R_x)/a_x\right]\}^{-1}$$

We will adopt the numerical values listed in table 3. In NRV, reduced radii are introduced. Then, these are converted internally to absolute (physical) radii using the projectile and target atomic numbers: $R_x = r_x(A_p^{1/3} + A_t^{1/3})$.

Figure 3 shows a screenshot of the OM parameters section in NRV, with the parameters already introduced. The application shows also the real and imaginary parts of the potential. In this case, we should get something similar to Fig. 4.

3.1 Numerical integration parameters

In addition to the optical potentials, we need to specify some additional parameters required for the numerical integration of the radial equation. Although the application sets some default values, it is convenient to check that the calculations are *converged* with respect to these parameters. In NRV, we need to specify the following numerical parameters:

- **Integration step (h):** This is the radial step used for the numerical integration of the differential equation (2). It has to be chosen smaller than the diffuseness of the potentials and than the characteristic wavelength of the projectile. A simple criterion is to set $hk \leq 0.2$, where k is the wave number associated with the kinetic energy. For example, for E_{lab}=22 MeV, $k = 2.01$ fm^{-1} and so $h \leq 0.2/2.01 = 0.1$ fm.

Figure 3: Optical parameters section of NRV.
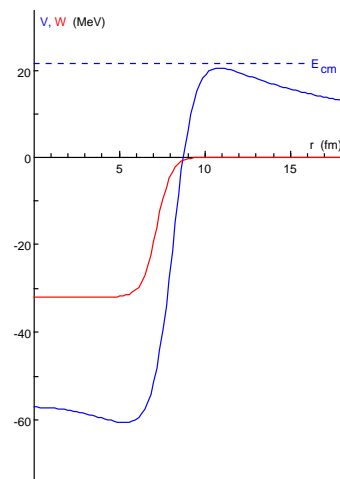
Figure 4: Real and imaginary parts of the optical potential, as displayed by the NRV application.

Figure 5: Numerical integration parameters section.

- **Maximum radius** $(R_{\max})$. This is the distance up to which the radial equations (2) are integrated. Beyond $R = R_{\max}$, the code will assume that all interactions (but the monopole Coulomb one) have vanished and so the wavefunction has reached its asymptotic behaviour, given by Eq. (3). Thus, $R_{\max}$ must be chosen well outside the range of the optical potential. In our example, this potential extends up to ≈ 10 fm. Clearly, $R_{\max}$ must be larger than the grazing distance (R_g) defined above which, in the present case is $R_g \simeq 1.45(4^{1/3} + 208^{1/3}) \approx 11$ fm.

  From these arguments, $R_{\max} \geq 20$ fm would be a "safe" choice in the present case.

- **Maximum angular momentum** $(L_{\max})$. In principle, the sum in L of Eq. (4) goes to infinity. In practice, convergence of the scattering observables is achieved for finite values of L since, for large values of L, $S_L \to 1$ and hence these values do not contribute to the sum (4). This occurs because, for large partial waves, the nuclear potential is negligible and the corresponding nuclear phase-shift tends to zero.

  Clearly, $L_{\max}$ must be larger than the "grazing" angular momentum (L_g), i.e., the value of L corresponding to a trajectory whose distance of closest approach is equal to the grazing distance $(r_{\min} = R_g)$. To get L_g from R_g, we consider the relation between the distance of closest approach r_{min} and the orbital angular momentum for a classical Coulomb trajectory, i.e.,

$$\sqrt{L(L+1)} \approx L + \frac{1}{2} = kr_{min} \left[1 - \frac{2\eta}{kr_{min}} \right]^{1/2}, \tag{11}$$

  and then we estimate L_g as the angular momentum for which $r_{min} = R_g$.

  When Coulomb is weak $(\eta \ll 1)$, we get the simpler relation

$$L_g + \frac{1}{2} \simeq kR_g, \tag{12}$$

  which tell us that the number of partial waves (that is, values of L) involved in the calculation scales as the square root of the kinetic energy. In practice, one can just increase progressively $L_{\max}$ until convergence of the studied observables is achieved.

E_{lab} (MeV)	E_{cm} (MeV)	k (fm^{-1})	η	r_{min} (fm)
5	4.91	0.960	23.1	48.1
10	9.81	1.36	16.3	24.1
22	21.6	2.01	11.0	10.9
27	26.5	2.23	9.94	8.9
60	58.9	3.32	6.67	4.0

Table 2: Useful kinematical parameters for the ^{4}He+^{208}Pb reaction at several incident energies. The parameters k, η and r_{min} correspond, respectively, to the wave number, the Sommerfeld parameter, and the distance of closest approach for a head-on collision.

4 Interpretation of the results

In Table 2 we list some kinematical parameters, namely, the wave number (k), the Sommerfeld parameter (η), and distance of closest approach in head-on Coulomb collision (r_{min}). These quantities can be computed with the expressions,

$$k = \sqrt{\frac{2\mu E_{\text{cm}}}{\hbar^2}}; \qquad \eta = \frac{Z_p Z_t e^2}{\hbar v} = \frac{Z_p Z_t e^2 \mu}{\hbar^2 k}; \qquad r_{\text{min}} = \kappa \frac{Z_1 Z_2 e^2}{E_{\text{cm}}}$$

where $\kappa = 1/(4\pi\epsilon_0)$. Note that this expression is more easily evaluated in a system of units with $\kappa = 1$.

4.1 Coulomb barrier

The nominal height of the Coulomb barrier can be estimated from the maximum of the real (Coulomb plus nuclear) potential. According to Fig. 4 we see that this is about 22 MeV. This is consistent with the simple estimate:

$$V_b \approx \frac{Z_1 Z_2 e^2}{R_b}; \qquad R_b \approx 1.44(A_1^{1/3} + A_2^{1/3}) \text{ fm}$$

which, in this case, gives $V_b \approx 21.8$ MeV and $R_b = 10.8$ fm.

4.2 Differential cross sections and S-matrix elements

The elastic differential cross section is shown in the upper panels of Fig. 6 for several incident energies: 10, 22, 27 and 60 MeV, plotted relative to the Rutherford cross section. In NRV, we can switch from absolute cross section using the option *View → mb/ratio* in the menubar. The associated S-matrix elements are shown in the lower panels of Fig. 6. From these graphs, we can notice the following features:

- At E=10 MeV, the ratio σ/σ_R is almost 1, that is, we are in a situation of **pure Coulomb scattering** and is well described by the Rutherford formula. At this energy, the projectile does not *feel* the nuclear interaction. This is consistent with

large value of $r_{\min}$ listed in Table 2. At this energy, the S-matrix is essentially 1 for all partial waves which corroborates the absence of absorption at this sub-Coulomb energy.

- At $E{=}22$ MeV, the distribution departs from the Rutherford formula, as a consequence of the nuclear interaction. Beyond a certain angle ($\theta_{\text{c.m.}} \approx 60°$), the cross section drops quickly. This is typical of the "shadow" region observed in diffraction that occurs in Fresnel scattering.

  As for modulus of the S-matrix, one sees that for the first L values, $|S_L| < 1$, due to the absorption produced by the imaginary part of the optical potential. Note that $|S_L|$ does not vanish completely at $L = 0$. This is usually referred to as "transparency".

- At $E{=}27$ MeV, the elastic angular distribution displays a typical **Fresnel** diffraction pattern. We recall that a prerequisite for the observation of this pattern is that $L_g \gg 1$ and $\eta \gg 1$. According to Table 2, at this energy $\eta = 8.9$, so the latter condition is fulfilled. The grazing angular momentum L_g can be estimated from the condition $|S_L| = 1/2$ which occurs for $L \simeq 10$.

  The grazing angle θ_g can be estimated from the quarter-point recipe: $\sigma/\sigma_R(\theta_g) = 1/4$, which gives $\theta_g \approx{=} 88.8°$. Then, using (9) we obtain the grazing angular momentum and grazing angle:

  $$L_g + 1/2 \approx \eta \cot\left(\frac{\theta_g}{2}\right) = 10.1 \quad \text{and} \quad R_g \approx \frac{\eta}{k}\left(1 + \frac{1}{\sin(\theta_g/2)}\right) = 10.8 \text{ fm}$$

  which agree very well with our former estimates.

- At $E{=}60$ MeV, the angular distribution displays a more oscillatory structure, departing from the Fresnel pattern and approaching to what we have called **Fraunhoffer** scattering.

By looking at the evolution of $|S_L|$ with the incident energy, we see that the range of values of L for which $|S_L| < 1$ increases for increasing energy. This can be understood as the increase of the grazing angular momentum with increasing incident energy, according to Eq. (12).

4.3   Near-side and far-side decomposition of the elastic cross section

In addition to the elastic cross section NRV provides also the *nearside* and *farside* components. In the optical model formalism, this can be realized by decomposing the Legendre polynomials appearing in the expansion of the scattering amplitude as

$$P_\ell(\cos\theta) \simeq \frac{e^{i\left((\ell+\frac{1}{2})\theta - \frac{\pi}{4}\right)} - e^{-i\left((\ell+\frac{1}{2})\theta - \frac{\pi}{4}\right)}}{\sqrt{2\pi\left(\ell+\frac{1}{2}\right)\cos\theta}} \quad \Rightarrow \quad f(\theta) = f^{\text{far}}(\theta) + f^{\text{near}}(\theta)$$

In Fig. 7 this decomposition is shown for the incident energies considered above. We can see that:
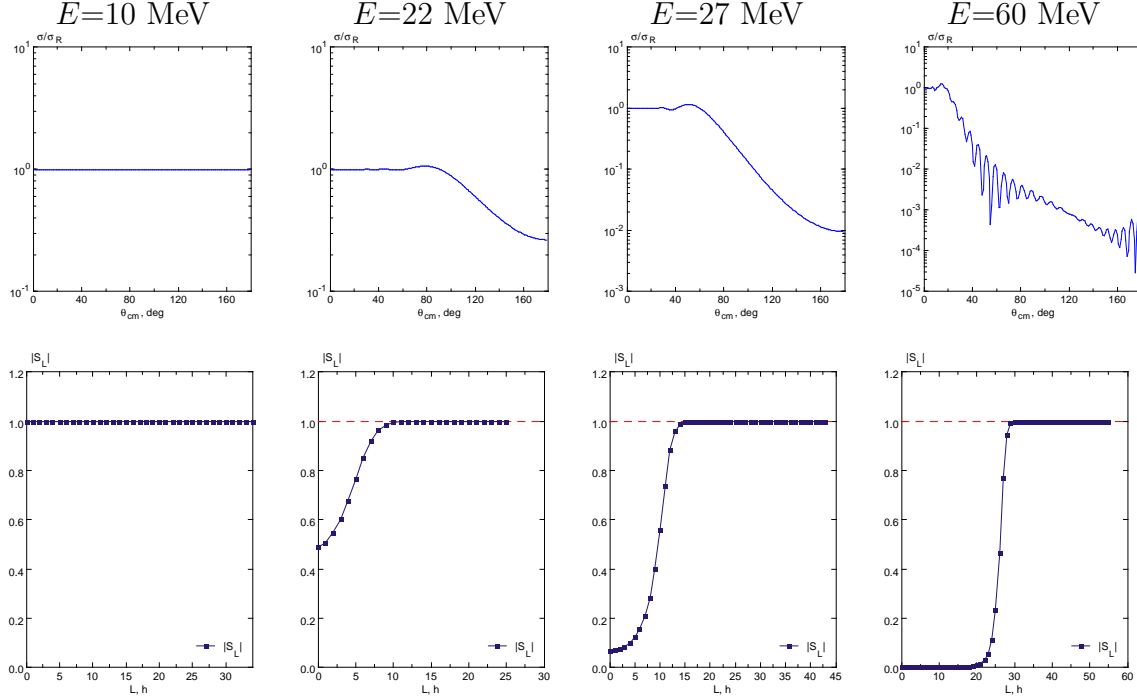
Figure 6: Top: Elastic differential cross sections relative to Rutherford cross section at E_{lab}=10, 22, 27 and 60 MeV (from left to right). Bottom: Modulus of the elastic S-matrix as a function of the total orbital angular momentum L.

- At 10 and 22 MeV, the cross section is almost entirely due to the nearside trajectories.

- At E=60 MeV, there are smooth regions dominated by either the *nearside* or the *farside* components. However, around $\theta_{\text{cm}} \approx 60°$ and $\theta_{\text{cm}} \approx 170°$ both components have similar magnitude, and their interference produces the observed oscillations in the elastic scattering.

5 Classical description

NRV allows also a classical treatment of the reaction. The code provides, among other quantities, the classical deflection function and the plot of the classical trajectories themselves for specific impact parameters.

Figure 8 depicts the deflection functions (top) and classical trajectories for a selected range of impact parameters (bottom) for the ^{4}He+^{208}Pb reaction at E_{lab}=10, 22 and 60 MeV. We see that:

- At 10 MeV (i.e., well below the barrier) the deflection function is a monotonously decreasing function of the impact parameter starting at $\Theta = 180°$ for $b = 0$ and tending to $\Theta = 0$ for large b. This is essentially the pure Coulomb deflection function.

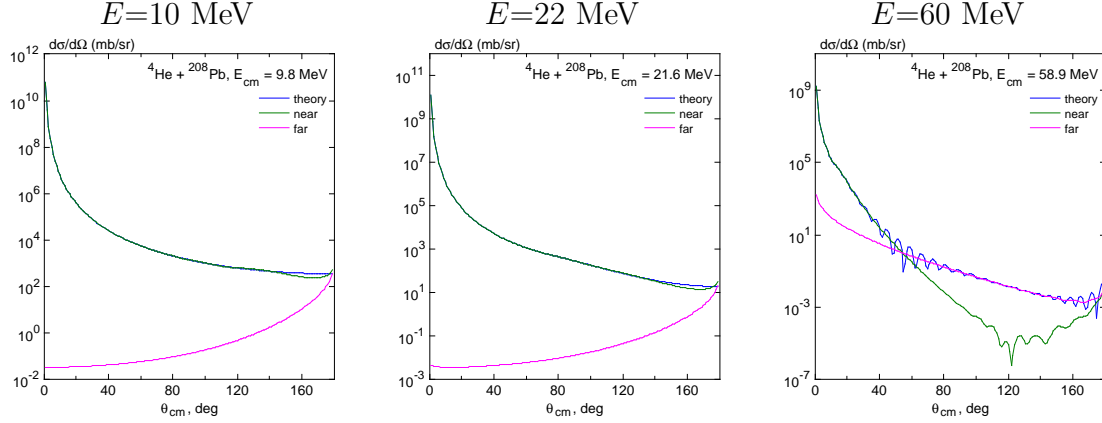Figure 7: Far-side /near-side decomposition of the elastic cross cross section ^{4}He+^{208}Pb at E_{lab}=10, 22 and 60 MeV.

- At $E_{\text{lab}} = 22$ MeV, the deflection function still follows the Coulomb deflection function for large impact parameters, reaches a maximum at $b = b_r \approx 2.5$ fm and then becomes negative for smaller impact parameters. This maximum corresponds to the **rainbow** region and is characterized by an accumulation of trajectories (i.e. impact parameters) leading to essentially the same scattering angle (the rainbow angle, θ_r), thus resembling the usual rainbow phenomenon.

  - For $b < b_r$, the deflection function is negative ($\Theta < 0$), thus corresponding to farside trajectories. The latter are dominated by the (attractive) nuclear interaction.

  - For $b = b_r$, $d\Theta/db = 0$ and hence $d\sigma/d\Omega \to \infty$ (that is, the classical cross section diverges at the rainbow angle).

  - For $\theta > \Theta_r$, the Coulomb trayectories and nuclear nearside trajectories do not contribute to the cross section. So, classically, there is a sharp decrease in the differential cross section for ($\theta > \Theta_r$). This is the **"shadow region"** appearing in Fresnel scattering.

- For $E = 60$ MeV, we see a similar pattern, but the region dominated by the nuclear interaction spans a larger number of impact parameters and the farside region is enhanced. An interesting phenomenon observed here is the **orbiting**: in the region for which the deflection function changes abruptly from positive to negative, a small variation on the impact parameter produces a large variation in the deflection function. In the vicinity of the orbiting impact parameter, $db/d\theta$ is very small, so orbiting has a very small impact on the cross sections.

6   Comparison with the ^{6}He+^{208}Pb case

The ^{6}He is an example of halo nucleus. As such, it is weakly-bound (the two-neutron separation energy is $S_{2n} \approx 1$ MeV) and its neutron distribution displays an extended
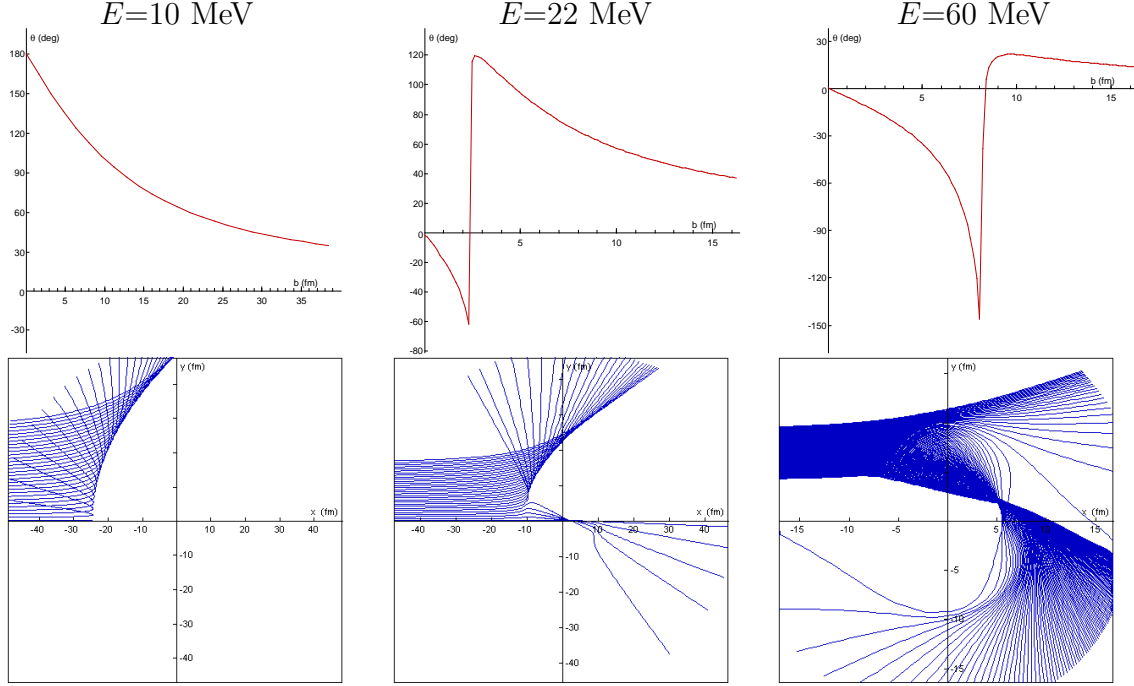
Figure 8: Deflection functions (top) and classical trajectories (bottom) for ^{4}He+^{208}Pb at E_{lab}=10, 22 and 60 MeV.

tail. This exotic structure manifests itself in the reaction observables, including elastic scattering. In Fig. 9 one can see the measured elastic scattering differential cross section measured at $E_{\text{lab}} = 22$ MeV, compared with two optical model calculations. The dashed-line corresponds to the optical model employed in the previous section for the ^{4}He+^{208}Pb case, which clearly deviates from the data. In particular, the calculation predicts a Fresnel-like pattern, whereas the data displays a monotonous decrease with the angle. The solid line is a fit of the data using the optical model parameters shown in the figure. In order to reproduce the data one needs a very diffuse imaginary part, which is indicative of long-range absorption effects taking place in this reaction. These are associated with the transfer/breakup modes leading to the dissociation of the halo neutrons and hence producing ^{4}He as a ejectile.
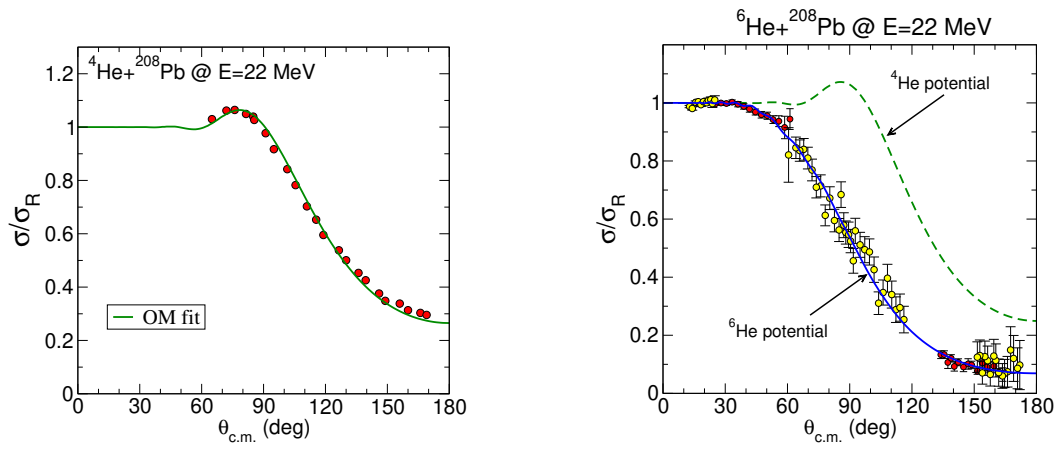
Figure 9: Elastic scattering of ^{4,6}He+^{208}Pb at $E_{\text{lab}} = 22$ MeV.